# Colloidal Synthesis and Optical Properties of All-inorganic $Cs_2CuCl_4$ Nanocrystals

Wanying Gu †, Yicheng Zeng †, Yuan Deng, Pan Huang, Geyu Jin, Fangze Liu, Jing Wei, Hongbo Li *

Posted Date: 8 May 2023

doi: 10.20944/preprints202305.0454.v1

Keywords: Cs2CuCl4 nanocrystals; Ag passivation; photoluminescence quantum yield; stability

*Article*

# Colloidal Synthesis and Optical Properties of All-Inorganic $Cs_2CuCl_4$ Nanocrystals

**Wanying Gu [1,†], Yicheng Zeng [1,†], Yuan Deng [1], Pan Huang [1], Geyu Jin [1], Fangze Liu [2], Jing Wei [1] and Hongbo Li [1,*]**

[1] School of Materials Science and Engineering, Beijing Institute of Technology, Beijing 100081, China

[2] Advanced Research Institute of Multidisciplinary Sciences, Beijing Institute of Technology, Beijing 100081, China

* Correspondence: hongbo.li@bit.edu.cn (H.L.)

† These authors have contributed equally to this work.

**Abstract:** Lead-free copper halide perovskite nanocrystals (NCs) are emerging materials with excellent photoelectric properties. Herein, we present a colloidal synthesis route of orthorhombic $Cs_2CuCl_4$ NCs with well-defined cubic shape and an average diameter of 24 ± 2.1 nm. The $Cs_2CuCl_4$ NCs exhibit bright deep blue photoluminescence, which is attributed to the Cu(II) defects. In addition, passivating the $Cs_2CuCl_4$ NCs by $Ag^+$ can effectively improve the photoluminescence quantum yield (PLQY) and environmental stability.

**Keywords:** $Cs_2CuCl_4$ nanocrystals; Ag passivation; photoluminescence quantum yield; stability

## 1. Introduction

Lead halide perovskites NCs with a general formula of $APbX_3$ (A=Cs, methylammonium and formamidinium, X=Cl, Br, I) have attracted great attention owing to their excellent photoelectric properties including high PLQY, high exciton binding energy, tunable PL emission wavelength and solution processability. They have shown great potentials in a variety of optoelectronic applications, such as solar cells [1], light-emitting diodes [2] and lasers [3]. At present, the external quantum efficiencies (EQEs) of red and green perovskite light-emitting diodes (PeLEDs) have exceeded 20%, reaching the industrial standard, but the EQE of blue PeLEDs is still lower than red and green PeLEDs [4–7]. This is mainly due to the deep level defects originated from the large band gap of blue-emitting materials.

Blue PeLEDs have been progressing significantly during the past few years. Zeng et al [8] first fabricated blue PeLEDs by using $CsPb(Cl/Br)_3$ NCs as blue emitters. However, the EQE was only 0.07% due to intrinsic phase instabilities of mixed-halide perovskites. Subsequently, Bakr et al [9] used n-dodecylammoniumthiocyanate (DAT) as a surface passivator to improve the PLQY of $CsPb(Cl/Br)_3$ NCs close to 100%, and therefore PeLEDs with EQE up to 6.3% were achieved. Although defects can be reduced through optimizations of synthesis conditions, they can still easily form during crystallization due to their low formation energy in chloride-based perovskite NCs. To increase the defect formation energy, metal doping has been shown as an effective strategy to obtain high quality perovskite NCs [10–12]. For example, Ni doping can improve the short-range order of the perovskite lattice of $CsPbCl_xBr_{3-x}$ NCs, and an EQE of 2.4% was obtained [10]. Mn ion is another effective dopant to increase the PLQY of perovskite NCs. Hou et al [11] carefully adjusted the concentration of Mn doping in $CsPbCl_xBr_{3-x}$ NCs to increase the PLQY by over threefold while the pure emission at 470 nm was maintained. As a result, the EQE of blue LEDs reached up to 2.1%.

Despite of the rapid development of blue PeLEDs based on lead halide perovskites, their further applications are hindered by the toxicity of lead. Therefore, lots of efforts have been devoted to reduce or substitute lead with less or nontoxic metals. For example, $Sb^{3+}$ and $Bi^{3+}$ ions can form $Cs_3M(III)_2X_9$ (M=Sb or Bi) structures [13–15]. These perovskites generally exhibit deep blue emission and high air

 doi:10.20944/preprints202305.0454.v1



stability. In addition, $Ag^+$ have been shown to be able to improve the PLQY of $Cs_3Bi_2Br_9$ NCs through reducing the surface trap density [14]. Cu is another promising alternative of lead by forming Cu based perovskites [16–18]. Deep blue PeLEDs based on zero-dimensional (0D) $Cs_3Cu_2I_5$ NCs have shown a high EQE of 1.12%, which was comparable to the best-performing deep blue PeLEDs based on lead halide perovskites [16].

However, the development of chloride based deep blue lead free PeLEDs is still far behind Br/I based green/red PeLEDs [19]. Recently, Yang et al [20] firstly reported the synthesis of $Cs_2CuX_4$ (X=Cl, Br, and Br/I) spherical quantum dots with blue-green emission by using an improved ligand-assisted reprecipitation technique at room temperature. By changing the halide composition and precursor ratios, the emission peak can be tuned from 385 nm to 504 nm. In order to solve the low solubility of CsBr and CsCl in polar solvents, Kar et al [21] used water as a solvent to synthesize square-shaped $Cs_2CuCl_4$ nanoplates with deep blue PL at 434 nm. Although the synthesis and optical properties of cesium copper(II) halide NCs have been reported, the preparation of colloidal $Cs_2CuCl_4$ NCs with high quality remains a challenge. Herein, we developed a synthesis of 0D $Cs_2CuCl_4$ NCs and examined its optical properties. The colloidal $Cs_2CuCl_4$ NCs have uniform size and excellent optical properties. We find that $Cs_2CuCl_4$ NCs have a wide band gap of 4.36 eV and show bright deep blue PL at 434 nm with a PLQY of 28.8% at room temperature. In addition, we show that the PLQY of $Cs_2CuCl_4$ NCs can be greatly improved to 42% by $Ag^+$ passivation. The air stability of $Ag^+$ treated $Cs_2CuCl_4$ NCs were also greatly improved. After 15-days storage in air (average temperature 25℃, humidity 50%), 75% of their initial PLQY was retained.

## 2. Materials and Methods

### *2.1. Materials*

Cesium acetate (Cs(OAc), 99.9%), Copper(II) acetate ($Cu(ac)_2$, 99.9%), silver acetate (Ag(ac), 99.99%), benzoyl chloride (Bz-Cl, 98%) and benzoyl bromine (Bz-Br, 99%) were purchased from Aladdin. 1-octadecene (ODE, 90%), oleylamine (OLA, 70%) and oleic acid (OA, 90%) were purchased from Sigma-Aldrich. All the chemicals and solvents were used without further purification.

### *2.2. Preparation of Ag-OLA solution*

Ag(ac) (25 mg) was loaded into a 50 mL three-neck flask along with ODE (10 mL) and OLA (1 mL). The mixture was degassed for 0.5 h at 30 ℃ until the Ag(ac) dissolved completely.

### *2.3. Synthesis of $Cs_2CuCl_4$ NCs*

In a typical synthesis, Cs(OAc) (13.4 mg), $Cu(ac)_2$ (18.2 mg), OA (1 ml), OLA (0.5 ml) and ODE (5 ml) were mixed in a 50 mL flask and dried for 30 min under vacuum at 100 °C. Then the reaction flask was heated to 120 ℃ in $N_2$ atmosphere, when 48 ul Bz-Cl dispersed in 0.5 ml of degassed ODE were injected inside the flask. After 10 s, the solution was cooled down using an ice-water bath. The resulting mixtures of $Cs_2CuCl_4$ NCs were centrifuged for 5 min at 8000 rpm. The precipitate was redissolved in hexane and centrifuged at 8000 rpm for 5 min to remove undissolved species. The final supernatant was collected for further analysis.

### *2.4. Synthesis of the Ag passivation reagent*

For absorption and PL spectra of NCs before and after Ag passivation, the as-prepared $Cs_2CuCl_4$ NCs (200 μL) were mixed with hexane (3 mL) in the cuvette, and then different amounts of Ag-OLA solution were injected and stirred for 2 min.

## 3. Results and Discussion

In this approach, $Cs_2CuCl_4$ NCs were synthesized using a modified hot-injection method. Figure 1a shows the crystal structure of $Cs_2CuCl_4$, where isolated tetrahedral $CuCl_4^{2-}$ unit are separated by the surrounding $Cs^+$ ions. Working with Cs/Cu/Cl molar ratio of 0.7/1/4, a pure $Cs_2CuCl_4$ phase was

Preprints (www.preprints.org) | NOT PEER-REVIEWED | Posted: 8 May 2023 doi:10.20944/preprints202305.0454.v1



observed by X-ray diffraction (XRD) analysis. The corresponding XRD pattern (Figure 1b) confirming that the obtained sample $Cs_2CuCl_4$ NCs has orthorhombic crystal system. Figure 1c show a typical large scale transmission electron microscopy (TEM) image indicate a uniform size distribution of the as-prepared colloidal $Cs_2CuCl_4$ NCs. The $Cs_2CuCl_4$ NCs are cubic structure with an average size of 24 ± 2.1 nm.

The UV/Vis absorption spectrum of $Cs_2CuCl_4$ NCs are presented in Figure 1d. The $Cs_2CuCl_4$ NCs shows a strong excitonic absorption peak at around 268 nm. Besides, the band gap of the $Cs_2CuCl_4$ NCs was measured by using the direct band gap tauc plot in Figure 1e, which shows 4.36 eV band gap for $Cs_2CuCl_4$ NCs. The PL spectrum (Figure 1d) of deep blue $Cs_2CuCl_4$ NCs exhibit emission peak at 434 nm (PLQY=28.8%) with a full width at half-maximum (FHWM) of roughly 58 nm, which matched with $Cs_2CuCl_4$ nanoplates [21]. The inset shows that $Cs_2CuCl_4$ NCs has excellent luminescence performance that strong deep blue emission under ultraviolet irradiation. The PL excitation (PLE) spectrum (monitoring emission at 434 nm) had a peak at 270 nm. The PLE spectrum matched with the exciton peak in the absorption spectrum, showing an apparent exciton characteristic of $Cs_2CuCl_4$ NCs. The luminescence origin of NCs was studied by monitoring the PL spectra at different excitation wavelengths. The Figure 1f showed that PL spectra excited at different wavelength have the same characteristics, indicating that the emission originates from the same excited state relaxation.

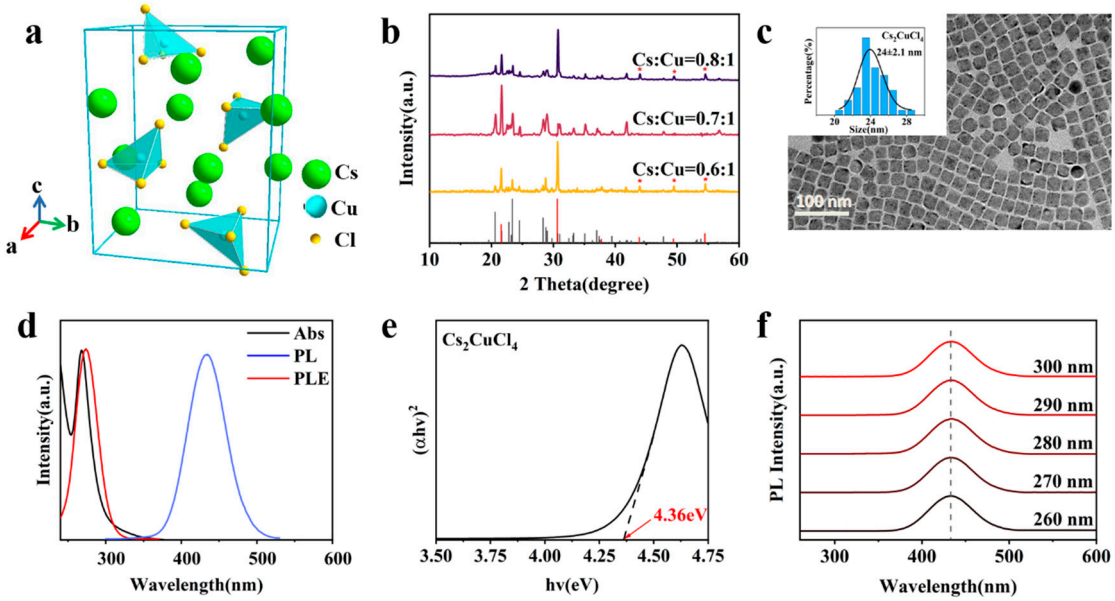


**Figure 1.** (a) Schematic crystal structure of $Cs_2CuCl_4$ NCs; (b) XRD pattern of $Cs_2CuCl_4$ NCs synthesized with different ratios of Cs:Cu (0.6:1, 0.7:1, 0.8:1). The red line at the bottom represents pure CsCl phase (PDF#05-06-07), and the black line at the bottom represents pure $Cs_2CuCl_4$ phase (PDF#71-09-01); (c) TEM image of $Cs_2CuCl_4$ NCs. The insets show the size distribution; (d) UV-Vis absorption, PLE, and PL spectra of $Cs_2CuCl_4$ NCs. Inset: photographs of $Cs_2CuCl_4$ NCs under ambient light (left) and 254 nm UV light excitation (right); (e) Tauc plot of UV-Vis absorption of $Cs_2CuCl_4$ NCs; (f) PL spectra of $Cs_2CuCl_4$ NCs excited at different wavelengths (260 nm to 300 nm).

We employed X-ray photoelectron spectroscopy (XPS) to examined the valence state of Cu in the $Cs_2CuCl_4$ NCs. Figure 2a displays the XPS survey spectrum in the entire binding energy region of the aggregated $Cs_2CuCl_4$ NCs, confirming the presence of $Cs^+$, $Cu^{2+}$ and $Cl^-$ elements at the surface. The satellite peak in the narrow scan of Cu 2p spectrum in Figure 2c indicates the presence of $Cu^{2+}$ ions on the surface of $Cs_2CuCl_4$ NCs [23].

Preprints (www.preprints.org) | NOT PEER-REVIEWED | Posted: 8 May 2023 doi:10.20944/preprints202305.0454.v1



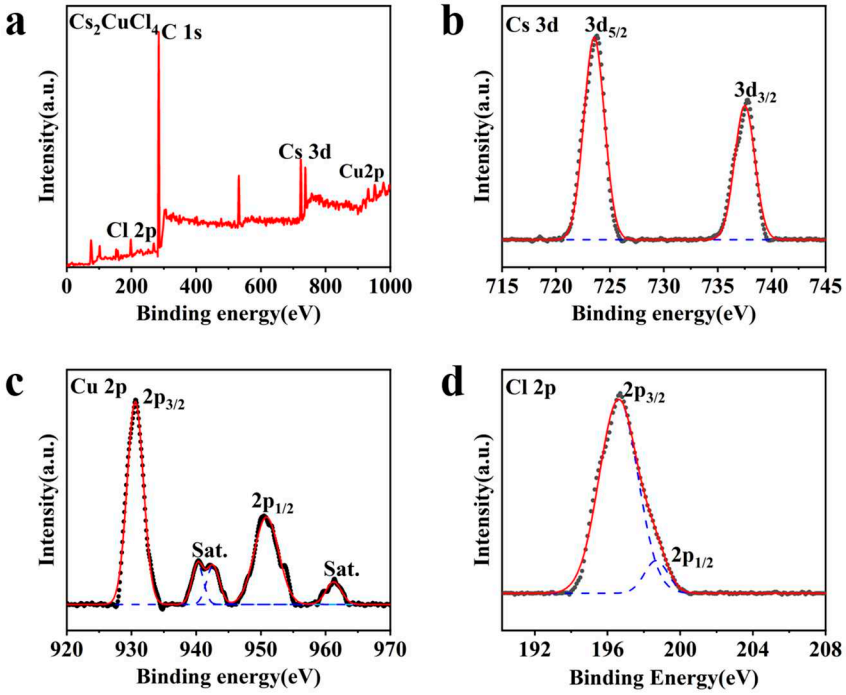


**Figure 2.** (a) XPS spectrum of $Cs_2CuCl_4$ NCs; (b, c, d) The high-resolution XPS spectra corresponding to Cs 3d, Cu 2p and Cl 2p, respectively.

The injection temperature is critical to the successful synthesis of $Cs_2CuCl_4$ NCs. Strong reducibility of oleylamine can easily reduce Cu(II) to Cu(I), while chlorine helps to stabilize the oxidation state of $Cu^{2+}$, which was proved by XPS spectra [22]. However, when benzoyl bromine is used as halide precursor, the presence of bromine will promote the reduction of $Cu^{2+}$ to $Cu^{+}$, then form $Cs_3Cu_2Br_5$ instead of $Cs_2CuBr_4$ with a peak position of 454 nm [18] (Figure S1). Although high injection temperature can reduce the surface defects of NCs, the Cu(II) will be reduced to Cu(I) by oleylamine when the temperature is too high. Therefore, the highest PLQY was obtained by optimizing the experimental scheme to get an optimal injection temperature. In Figure 3a and Figure 3b, the optimal injection temperature is found to be 120℃ by comparing the UV/Vis absorption spectrum and PL spectra of $Cs_2CuCl_4$ NCs synthesized at different injection temperatures.

Beside temperature, the molar ratio of Cs and Cu precursors as well as the ratio of OA and OLA are also important parameters for the synthesis of high-quality $Cs_2CuCl_4$ NCs. With Cs/Cu molar ratio of 0.7:1, we observed the formation of pure phase of $Cs_2CuCl_4$ NCs with narrow size distribution and high PLQY (Figure 3c-d). However, a molar ratio of 0.6:1 or 0.8:1 lead to reduced PLQY of $Cs_2CuCl_4$ NCs due to the presence of CsCl impurity phase, which was confirmed by the XRD pattern in Figure 1b. In addition, the ratio between OA and OLA can also affect the surface defect and stability of $Cs_2CuCl_4$ NCs. We found the optimal amount of OA and OLA was 1.0 ml and 0.5 ml, respectively (see Experimental section), which resulted in the lowest surface defects density of $Cs_2CuCl_4$ NCs (Figure 3f). The presence of OA and OLA ligands were further confirmed by Fourier infrared spectroscopy (FITR) (Figure S2) [21]. The peak at 1470 $cm^{-1}$ represents the $COO^-$ stretching vibration mode of OA. The peak at 1720 $cm^{-1}$ represents the asymmetric vibration mode of OA. The peak at 2855 $cm^{-1}$, 2905 $cm^{-1}$ represents the vibration due to the stretching of the C-H bonds of $-CH_3$ and $-CH_2$ in the aliphatic hydrocarbon chain. The peak at 1624 $cm^{-1}$ represents the bending vibration of N-H scissors of $-NH_2$ group in OLA. The above results represent the stable existence of OA and OLA ligands on $Cs_2CuCl_4$ NCs surface.

Preprints (www.preprints.org) | NOT PEER-REVIEWED | Posted: 8 May 2023 doi:10.20944/preprints202305.0454.v1



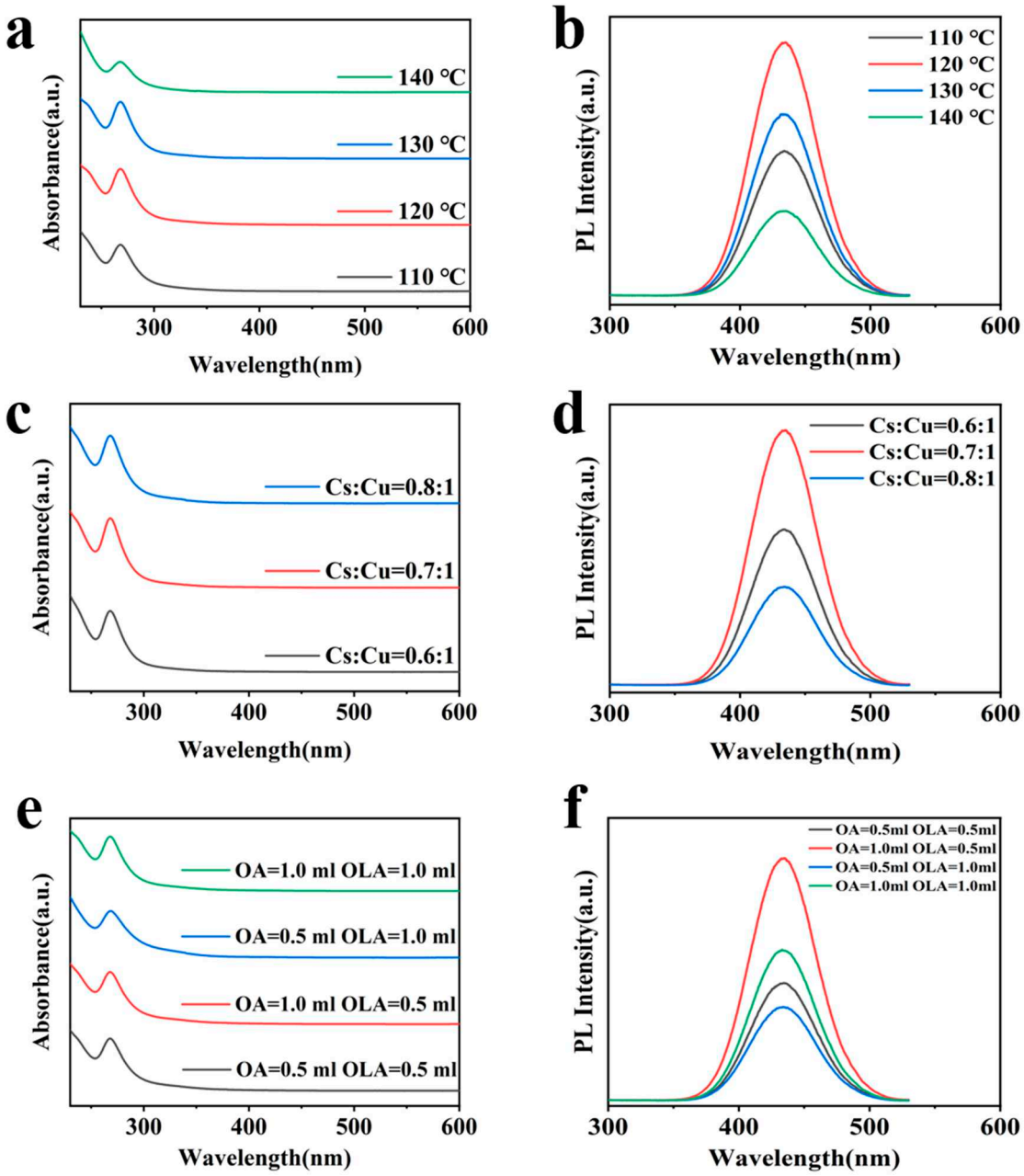


**Figure 3.** (a) UV/Vis absorption, (b) PL spectra of $Cs_2CuCl_4$ NCs under different injection temperatures (110℃, 120℃, 130℃, 140℃); (c) UV/Vis absorption, (d) PL spectra of $Cs_2CuCl_4$ NCs synthesized with different ratios of Cs:Cu (0.6:1, 0.7:1, 0.8:1); (e) UV/Vis absorption, (f) PL spectra of $Cs_2CuCl_4$ NCs synthesized with different amounts of OA:OLA (1 ml:1 ml, 0.5 ml:1 ml, 1 ml:0.5 ml, 0.5 ml:0. 5ml).

Passivation of NCs with Ag to reduce surface defects is an effective method to improve PLQY. For example, Li et al [23] treated $CsPbBr_3$ NCs using Ag-trioctylphosphine complex to reduce surface defects and improve the PLQY of $CsPbBr_3$ NCs significantly. Here, the Ag-OLA solution was added for surface passivation treatment of $Cs_2CuCl_4$ NCs. We found a small amount of Ag-OLA solution can effectively bound chloride on the $Cs_2CuCl_4$ NCs surface, reducing the surface traps caused by the loss of unstable ammonium chloride. Different amounts of Ag-OLA solution were added into 3 mL $Cs_2CuCl_4$ NCs colloidal solution, and the absorption (Figure 4a) and PL spectra (Figure 4b) were measured 2 min later. Compared with untreated sample, the absorbance of Ag treated $Cs_2CuCl_4$ NCs increased slightly, but the peak position remained unchanged for different amounts of Ag-OLA. The PLQY of Ag-treated sample reached maximum value of 42% with adding 15 ul Ag-OLA, which is

Preprints (www.preprints.org) | NOT PEER-REVIEWED | Posted: 8 May 2023 doi:10.20944/preprints202305.0454.v1



nearly 70% higher than that of untreated sample. In addition, we studied the air stability of Ag-treated $Cs_2CuCl_4$ NCs in ambient environment (average temperature 25℃, humidity 50%). As shown in Figure 4d, the PLQY of Ag-treated $Cs_2CuCl_4$ NCs maintained ~75% of their initial PLQY after 15 days storage period, while the PLQY of untreated NCs decreased to 1% of their initial value, demonstrating the excellent stability of the Ag-treated $Cs_2CuCl_4$ NCs. Importantly, as shown in Figure S3, individual OLA cannot increase the fluorescence intensity of $Cs_2CuCl_4$ NCs, proving that Ag plays a key role in enhancing the PLQY of $Cs_2CuCl_4$ NCs. The existence of Ag on the surface of $Cs_2CuCl_4$ NCs was verified by XPS shown in Figure 4e, where the Ag peaks can be clearly seen from the Ag-treated $Cs_2CuCl_4$ NCs. Figure 4f indicating that Ag exists on the surface of $Cs_2CuCl_4$ NCs in the form of Ag (I) in the oxidation state. The Ag-treated NCs present regular cubic shape and size distributions at Figure 4g, with little change compared with the untreated ones.

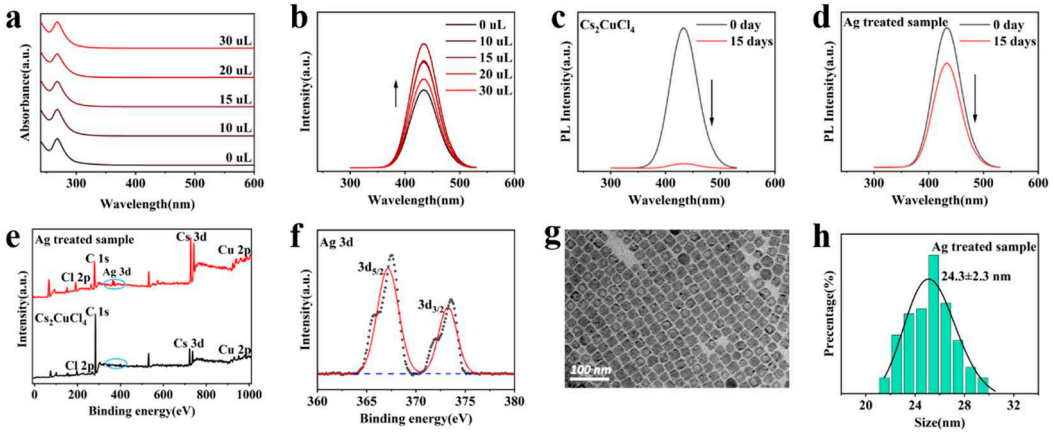


**Figure 4.** (a) Absorption spectra of $Cs_2CuCl_4$ NCs and Ag-treated samples dispersed in hexane by adding different volume of Ag-OLA reagent. (b) The evolution of PL spectra of Ag-treated $Cs_2CuCl_4$ NCs. Highest PL was achieved by adding 15 ul Ag-OLA. Changes in PL intensity of (c) $Cs_2CuCl_4$ NCs and (d) Ag treated sample after 15 days of storage, demonstrating the excellent stability of Ag-treated sample. (e) XPS spectrum of $Cs_2CuCl_4$ NCs before and after Ag treatment. The Ag peaks can be clearly seen. (f) High-resolution Ag 3d spectrum of Ag-treated samples indicates the Ag(I) state. (g) TEM image of the Ag-treated $Cs_2CuCl_4$ NCs. (h) Size distribution histogram of the Ag-treated $Cs_2CuCl_4$ NCs.

The origin of bright blue emission of $Cs_2CuCl_4$ NCs can be attributed to the Cu ion induced traps. Manna et al [24] found doping $Cu^+$ into $Cs_2ZnCl_4$ NCs can achieve bright blue emission due to that the Cu(I) ions can promote the formation of trapped excitons. In addition, Xu et al [25] proposed that the emission from Cu-doped ZnO nanorods originates from Cu(II) defect. Therefore, we propose the schematic model of the luminescence mechanism of $Cs_2CuCl_4$ NCs in Figure S4. Under UV light excitation, electrons transition from the ground state to the photoexcited state, and then undergo a non-radiative compound transition to the $Cu^{2+}$ defect state. The electrons at the defect level transition back to the ground state as a radiative recombination, exhibiting a broad spectrum of deep blue luminescence.

## 4. Conclusions

We successfully synthesized pure phase $Cs_2CuCl_4$ NCs with well-defined shapes via a modified hot-injection synthesis strategy. With optimized injection temperature, precursor and ligand ratios, the $Cs_2CuCl_4$ NCs showed high PLQY (28.8%) in the deep blue spectrum at 434 nm. The PLQY and stability of $Cs_2CuCl_4$ NCs can be further enhanced through Ag treatment, where Ag-treated $Cs_2CuCl_4$ NCs exhibit higher PLQY (42%) and better air stability in ambient environment. This work provides a useful strategy for the synthesis of Cu(II) based metal halide perovskite NCs, which are promising materials to reduce the toxicity and realize practical application of perovskite NCs for display and lighting devices.

**Supplementary Materials:** The following supporting information can be downloaded at the website of this paper posted on Preprints.org.

**Author Contributions:** Conceptualization, H.L.; Methodology, W.G.; Data curation, Y.Z.; Writing—original draft preparation, W.G. and Y.Z.; Writing—review and editing, H.L. and F.L.; Resources, Y.D.; P.H. and G.J. All authors have read and agreed to the published version of the manuscript.

**Funding:** This research was funded by the National Natural Science Foundation of China (22179009, 22105018, 22005034).

**Data Availability Statement:** Not applicable.

**Conflicts of Interest:** The authors declare no conflict of interest.

## References

1. Ling, X.; Zhou, S.; Yuan, J.;Shi, J.; Qian, Y.; Larson, B. W.; Zhao, Q.; Qin, C.; Li, F.; Shi, G.; Stewart, C.; Hu, J.; Zhang, X.; Luther, J. M.; Duhm, S.; Ma, W. 14.1% $CsPbI_3$ Perovskite Quantum Dot Solar Cells via Cesium Cation Passivation. Adv. Energy Mater. 2019, 9, 1900721.
2. Li, C.; Zhou, Z.; Vashishtha, P.; Halpert, J. E. The Future Is Blue (LEDs): Why Chemistry Is the Key to Perovskite Displays. Chem. Mater. 2019, 31, 6003−6032.
3. Zhu, H.; Fu, Y.; Meng, F.; Wu, X.; Gong, Z.; Ding, Q.; Gustafsson, M. V.; Trinh, M. T.; Jin, S.; Zhu, X. Y. Lead Halide Perovskite Nanowire Lasers with Low Lasing Thresholds and High Quality Factors. Nat. Mater. 2015, 14, 636−642.
4. Kim, Y. H.; Kim, S.; Kakekhani, A.; Park, J.; Park, J.; Lee, Y. H.; Xu, H.; Nagane, S.; Wexler, R. B.; Kim, D. H.; Jo,S. H.;Sarti, L. M.; Tan, P.; Sadhamala, A.;Park, G. S.; Kim, Y. W.; Hu, B.; Bolink, H. J.; Yoo, S.; Friend, R. H.; Rappe, A. M., Lee, T. W. Comprehensive defect suppression in perovskite nanocrystals for high-efficiency light-emitting diodes. Nat. Photonics. 2021, 15, 148−155.
5. Zhu, L.; Cao, H.; Xue, C.; Zhang, H.; Qin, M.; Wang, J.; Wen, K.; Fu, Z.; Jiang, T.; Xu, L.; Zhang, Y.; Cao, Y.; Tu, C.; Zhang, J.; Liu, D.; Zhang, G.; Kong, D.; Fan, N.; Li, G.; Yi, C.; Peng, Q.; Chang, J.; Lu, X.; Wang, N.; Huang, W.; Wang, J. Unveiling the additive-assisted oriented growth of perovskite crystallite for high performance light-emitting diodes. Nat. Commun. 2021, 12, 5081.
6. Zhou, Y. H.; Wang, C.; Yuan, S.; Zou, C.; Si, Z.; Wang, K.; Xia, Y.; Wang, B.; Di, D.; Wang, Z. K.; Liao, L.S. J. Am. Chem. Soc. 2022, 144, 18470−18478.
7. Zhang, C.; Wan, Q.; Ono, L.K.; Liu, Y.; Zheng, W.; Zhan, Q.; Liu, M.; Kong, L.; Li, L.; Qi, Y.; ACS Energy Lett. 2021, 6, 3545−3554.
8. Song, J.; Li, J.; Li, X.; Xu, L.; Dong, Y.; Zeng, H. Quantum Dot Light-Emitting Diodes Based on Inorganic Perovskite Cesium Lead Halides ($CsPbX_3$). Adv. Mater. 2015, 27, 7162−7167.
9. Zheng, X.; Yuan, S.; Liu, J.; Yin, J.; Yuan, F.; Shen, W. S.; Yao, K.; Wei, M.; Zhou, C.; Song, K.; Zhang, B. B.; Lin, Y.; Hedhili, M. N.; Wehbe, N.; Han, Y.; Sun, H. T.; Lu, Z. H.; Anthopoulos, T. D.; Mohammed, O. F.; Sargent, E. H.; Liao, L. S.; Bakr, O. M. Chlorine Vacancy Passivation in Mixed Halide Perovskite Quantum Dots by Organic Pseudohalides Enables Efficient Rec. 2020 Blue Light-Emitting Diodes. ACS Energy Lett. 2022, 5, 793−798.
10. Pan, G.; Bai, X.; Xu, W.; Chen, X.; Zhai, Y.; Zhu, J.; Shao, H.; Ding, N.; Xu, L.; Dong, B.; Mao, Y.; Song, H. Bright Blue Light Emission of $Ni^{2+}$ Ion-Doped $CsPbCl_xBr_{3-x}$ Perovskite Quantum Dots Enabling Efficient Light-Emitting Devices. ACS Appl. Mater. Interfaces. 2020, 12, 14195−14202.
11. Hou, S.; Gangishetty, M. K.; Quan, Q.; Congreve, D. N. Efficient Blue and White Perovskite Light-Emitting Diodes via Manganese Doping. Joule. 2018, 2, 2421−2433.
12. Locardi, F.; Cirignano, M.; Baranov, D.; Dang, Z.; Prato, M.; Drago, F.; Ferretti, M.; Pinchetti, V.; Fanciulli, M.; Brovelli, S.; Trizio, L. D.; Manna, L. Colloidal Synthesis of Double Perovskite $Cs_2AgInCl_6$ and Mn-Doped $Cs_2AgInCl_6$ Nanocrystals. J. Am. Chem. Soc. 2018, 140, 12989−12995.
13. Lou, Y.; Fang, M.; Chen, J.; Zhao, Y. Formation of highly luminescent cesium bismuth halide perovskite quantum dots tuned by anion exchange. Chem. Comm. 2018, 54, 3779−3782.
14. Li, T.; Ma, J.; Qiao, M.; Kuang, Y.; He, Y.; Ran, X.; Guo, L.; Wang, X. Enhanced blue photoluminescence and photostability of $Cs_3Bi_2Br_9$ perovskite quantum dots via surface passivation with silver ions. CrystEngComm. 2021, 23, 7219−7227.
15. Ma, Z.; Shi, Z.; Yang, D.; Zhang, F.; Li, S.; Wang, L.; Wu, D.; Zhang, Y.; Na, G.; Zhang, L.; Li, X.; Zhang, Y.; Shan, C.; Electrically-Driven Violet Light-Emitting Devices Based on Highly Stable Lead-Free Perovskite $Cs_3Sb_2Br_9$ Quantum Dots. ACS Energy Lett. 2020, 5, 385−394.
16. Wang, L.; Shi, Z.; Ma, Z.; Yang, D.; Zhang, F.; Ji, X.; Wamg, M.; Chen, X.; Na, G.; Chen, S.; Wu, D.; Zhang, Y.; Li, X.; Zhang, L.; Shan, C. Colloidal Synthesis of Ternary Copper Halide Nanocrystals for High-Efficiency Deep-Blue Light-Emitting Diodes with a Half-Lifetime above 100 h. Nano Lett. 2020, 20, 3568−3576.

17. Li, Y.; Zhou, Z.; Tewari, N.; Ng, M.; Geng, P.; Chen, D.; K, P. K.; Qammar, M.; Guo, L.; Halpert, J. E. Progress in copper metal halides for optoelectronic applications. Mater. Chem. Front. 2021, 5, 4796–4820.
18. Cheng, P.; Sun, L.; Feng, L.; Yang. S.; Yang, Y.; Zheng, D.; Zhao, Y.; Sang, Y.; Zhang, R.; Wei, D.; Deng, W.; Han, K. Colloidal Synthesis and Optical Properties of All-Inorganic Low-Dimensional Cesium Copper Halide Nanocrystals. Angew. Chem. Int. Ed. 2019, 58, 16087–16091.
19. Zhang, C.; Wan, Q.; Ono, L. K.; Liu, Y. Zheng, W.; Zhang, Q.; Liu, M.; Kong, L.; Li, L.; Qi, Y. Narrow-Band Violet-Light-Emitting Diodes Based on Stable Cesium Lead Chloride Perovskite Nanocrystals. ACS Energy Lett. 2021, 6, 3545–3554.
20. Yang, P.; Liu, G.; Liu, B.; Liu, X.; Lou, Y.; Chen, J.; Zhao, Y. All-inorganic $Cs_2CuX_4$ (X=Cl, Br, and Br/I) perovskite quantum dots with blue-green luminescence. Chem. Comm. 2018, 54, 11638.
21. Shankar, H.; Jha, A.; Kar, P. Water-assisted synthesis of lead-free Cu based fluorescent halide perovskite nanostructures. Mater. Adv. 2022, 3, 658–664.
22. Cortecchia, D.; Dewi, H. A.; Yin, J.; Bruno, A.; Chen, S.; Baikie, T.; Boix, P. P.; Gratzel, M.; Mhaisalkar, S.; Soci, C.; Mathews, N. Lead-Free $MA_2CuCl_xBr_{4-x}$ Hybrid Perovskites. Inorg. Chem. 2016, 55, 3, 1044–1052.
23. Li, H.; Qian, Y.; Xing, X.; Zhu, J.; Huang, X.; Jing, Q.; Zhang, W.; Zhang, C.; Lu, Z. Enhancing Luminescence and Photostability of $CsPbBr_3$ Nanocrystals via Surface Passivation with Silver Complex. J. Phys. Chem. C. 2018, 122, 12994–13000.
24. Zhu, D.; Zaffalon, M. L.; Pinchetti, V.; Brescia, R.; Moro, F.; Fasoli, M.; Fanciulli, M.; Tang, A.; Infante, I.; Trizio, L.D.; Brovelli, S.; Manna, L. Bright Blue Emitting Cu-Doped $Cs_2ZnCl_4$ Colloidal Nanocrystals. Chem. Mater. 2020, 32, 5897–5903.
25. Xu, C.; Sun, X.; Zhang, X.; Ke, L.; Chua, S. Photoluminescent properties of copper-doped zinc oxide nanowires. Nanotechnology. 2004, 15, 856.